Smart Materials and
Structures

PURPOSE-LED
PUBLISHING™

PAPER

Thermo-mechanical response of the twisted and coiled polymer actuator (TCPA): a finite element analysis (FEA)

To cite this article: Robert Hunt *et al* 2021 *Smart Mater. Struct.* **30** 065017

IOP Publishing
Smart Materials and Structures
Smart Mater. Struct. **30** (2021) 065017 (10pp)
https://doi.org/10.1088/1361-665X/abfb84

Thermo-mechanical response of the twisted and coiled polymer actuator (TCPA): a finite element analysis (FEA)

Robert Hunt, Zakai Olsen and Kwang Kim*

Active Materials and Smart Living (AMSL) Laboratory, Mechanical Engineering Department, University of Nevada, Las Vegas (UNLV), 4505 S. Maryland Pkwy, Las Vegas, NV 89154-4027, United States of America

E-mail: Kwang.kim@unlv.edu

Received 6 April 2021
Accepted for publication 26 April 2021
Published 11 May 2021

Abstract

Twisted and coiled polymer actuators (TCPAs) are a recently discovered thermally driven artificial muscle, fabricated from a polymer fiber coiled into a helix. They produce axial contraction or torsion when heated above glass transition temperature and relaxes to their previous state when cooled back to their initial temperature. Studies have shown the actuator to produce enormous tensile strain (49%), power densities (27.12 kW kg^{-1}), and specific work (2.48 kJ kg^{-1}) [Haines (2014 *Science* **343** 868–72)]. The remarkable capabilities of TCPAs have raised interest in the applications of smart materials, soft robotics, and artificial muscles. Recently, Yang *et al* investigated the physical phenomena of TCPA's actuation through a top-down multiscale model, validated through experimental works [Yang and Li (2016 *J. Mech. Phys. Solids* **92** 237–59)]. This paper extends Yang's approach to a finite element analysis simulation for predicting the thermo-mechanical response of a TCPA, validated by experimental comparison. Currently, there are little to no studies done in the numerical simulation of TCPAs, which is an essential tool in all fields of engineering. A numerical simulation is imperative for increasing the model's adaptability in real-life physical systems, where analytical solutions become too complex, and for predictive simulations for designing prototype robotic actuators. The equations developed by Yang *et al* are implement into a three-dimensional COMSOL Multiphysics model. The results of the numerical simulation displacement response show great accuracy when compared to the experimental data tested by a dynamic mechanical analyzer.

Keywords: twisted and coiled polymer actuators (TCPA), artificial muscle, actuation

(Some figures may appear in colour only in the online journal)

1. Introduction

TCPAs are a novel artificial muscle that produces torsional and tensile actuation when heated above the glass transition temperature. Its record-breaking energy density, tensile stroke, and simplicity have drawn great attention to TCPAs and increased research activity in recent years. Various testing methods have been employed to characterize the actuator's displacement, strain, stress, hysteresis, and repeatability [1, 3–8]. And, the applications of TCPAs are in the fields of artificial muscle and soft robotics fields [5–12]. Though highly investigated, there is little attention in the thermo-mechanical modeling of TCPA, let alone the numerical simulation.

The studies used to quantify the thermo-mechanical response use indirect and direct approaches. Phenomenological methods are commonly used to model TCPA [13] and

* Author to whom any correspondence should be addressed.

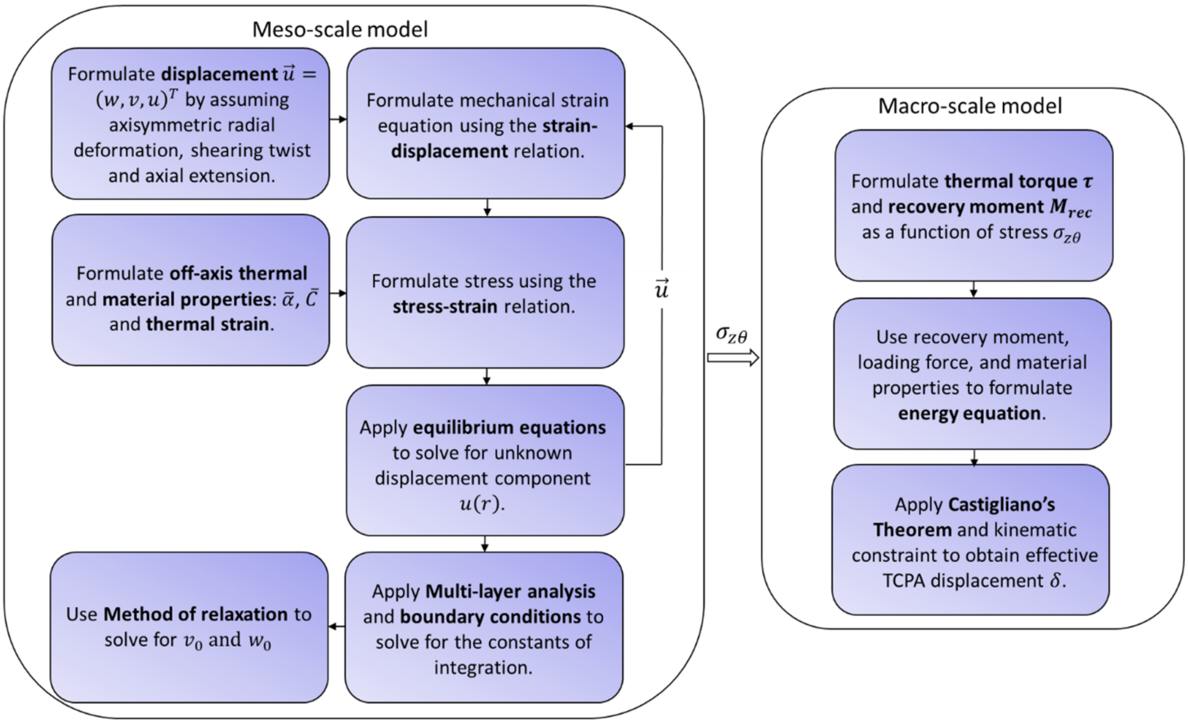

Figure 1. Flow chart for modeling the meso- and macro-scale model for attaining the thermo-mechanical response of the twisted and coiled polymer actuator.

are utilized in position control models [14–22], temperature control models [23], and hysteresis models [24]; however, implementation requires parameters to be experimentally identified, thus not capturing the correlation between the physical performance of the TCPA to the material and thermal properties. A study done by Sharafi and Li used a molecular-scale model to define the thermo-mechanical response of TCPA, however, the model is complex and difficult to implement. More recently, a fully developed model derived by Yang *et al* related the nano-, micro- and meso-scale to the overall tensile deformation in a top-down multi-scale model. The results were experimentally verified to confirm its accuracy [2]. The results of this study established a foundation of future TCPA models under an finite element analysis (FEA) formulation.

In this paper, Yang's model was utilized to develop a novel 3D FEA model of the thermo-mechanical response of TCPA to achieve a robust computationally efficient simulation using COMSOL Multiphysics. Developing an FEA simulation would greatly increase the adaptability of Yang's model for applications in soft robotics. FEA is a widely used tool in engineering. Applications of FEA are rooted in the aeronautical, automotive, and biomedical industries and have extended to all fields of engineering including soft robotics. FEA simulations are used for their modeling capability where complex geometries and irregular shapes can be integrated. It is highly adaptable, capable of meeting detailed specifications and design parameters iterated multiple times, and produces accurate visual-based solutions where vulnerabilities in the design are easily spotted. The goal of this study is to present an FEA model of TCPA that can be implemented in soft robotic applications for preliminary design analysis and optimization.

The paper is arranged as follows. In section 2, the meso-, and macro-scale equation derived by Yang *et al* are presented. In section 3, the model was implemented in COMSOL Multiphysics. The geometry was obtained by optical microscopy measurements of a fabricated TCPA. Curvilinear coordinates were developed in COMSOL for applying the material and thermal properties of the TCPA. A prescribed temperature was applied to the surface of the TCPA resulting in a thermo-mechanical response. In section 4, a TCPA was fabricated and the thermo-mechanical displacement response was experimentally measured by a dynamic mechanical analyzer (DMA). In section 5, the simulation is compared to the experimental results and the concluding remarks and future works are made in section 6.

2. Physics-based model

The constitutive equations developed by Yang *et al* are used to describe the tensile actuation of the TCPA. Previous work done by Haines suggested that the torsional actuation induced by heat is the underlying cause of the large tensile actuation. The torsional actuation was modeled on the meso-scale using an analysis of a cylindrical laminate formulated by Pipes *et al.* It was then related to the macro-scale displacement δ using an energy equation and Castigliano's Theorem. A flowchart of the thermo-mechanical modeling is shown in figure 1. The model presented as followed: the macro-scale energy equation

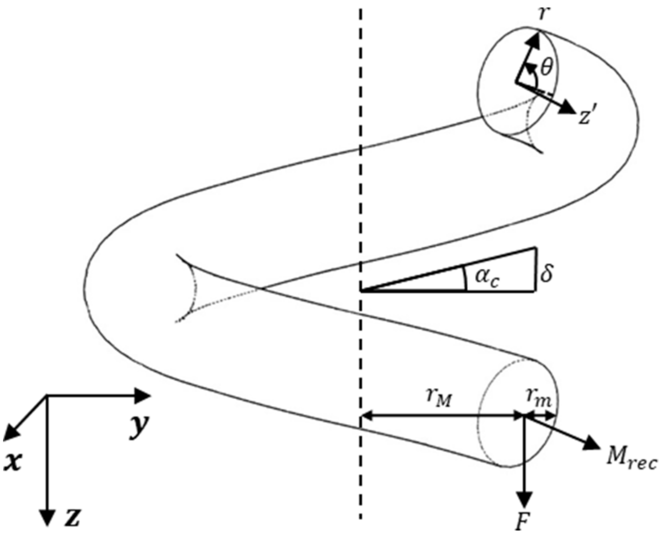

Figure 2. Force body diagram of a TCPA with an applied loading force F and the resulting recovery moment M_{rec} caused by thermal expansion. Two reference frames are displayed, the local cylindrical coordinates (z', θ, r) and the global cartesian (x, y, z).

is formulated and Castigliano's equation is applied for TCPA displacement. The recovery moment is then formulated as a function of stress, and the stress component is derived using the meso-scale model using a continuum mechanics approach.

The macro-scale (figure 2) energy equation is [2]

$$U = \int_0^{L_c} \left(\frac{M_z^2}{2\bar{G}J} + \frac{M_\theta^2}{2\bar{E}I} + \frac{F_z^2}{2\bar{E}A} + \frac{F_\theta^2}{2\bar{G}A} \right) \mathrm{d}l \tag{1}$$

where $\bar{E}$ and $\bar{G}$ are the effective moduli of the twisted fiber, $J = \frac{\pi r_{\text{m}}{}^4}{2}$ is the polar moment of area, $I = \frac{\pi r_{\text{m}}{}^4}{4}$ is the second moment and $A = \pi r_{\text{m}}^2$ is the cross-sectional area of the fiber and r_{m} is the polymer fiber radius or minor radius. $F_z = F\sin\alpha_c$, $F_\theta = F\sin\alpha_c$, $M_Z = -Fr_{\text{m}}\cos\alpha_c + M_{\text{rec}}$ and $M_\theta = Fr_{\text{m}}\sin\alpha_c$ are the forces and moments in the local cylindrical coordinate frame caused by the loading force F and the recover moment M_{rec} induced by thermal expansion decomposed into components based on the bias angle α_c and the moment arm r_M, the distance from the center of the coil to the center of the polymer fiber or major radius. The simplified energy equation is

$$U = \frac{1}{2} f_{11} F^2 - 2 f_{12} F M_{\text{rec}} + \frac{1}{2} f_{22} M_{\text{rec}}^2 \tag{2}$$

where f_{11}, f_{12}, and f_{22} are the collected constants. The parameters for the macro-scale model are provided in table 1. The displacement of the TCPA can be found using Castigliano's theorem [2, 25–27].

$$\delta = \frac{\mathrm{d}U}{\mathrm{d}F}. \tag{3}$$

The displacement is also related the kinematic relation [2].

$$\delta = L_c \sin\alpha_{\text{c}} - L_{c0} \sin\alpha_{c0}. \tag{4}$$

Table 1. Macro-scale parameters.

Parameter	Description
α_{c_0}	TCPA initial bias angle (rad)
F	Loading force (F)
L_{c_0}	TCPA initial fiber length (m)
r_{M}	Major radius (m)
r_{m}	Minor radius (m)
T	Temperature (°C)

Using equations (2)–(4), the pitch angle α_{c} and displacement δ can be expressed in terms of $\bar{E}$, $\bar{G}$, d and M_{rec}. The temperature induced recovery moment M_{rec} was formulated by integrating the recovery torque at each temperature step and the recovery torque was formulated by integrating the shearing stress $\sigma_{z\theta}$ over the cross-sectional area of the polymer fiber, where the stress component $\sigma_{z\theta}$ is derived in the meso-scale [2, 25–27].

$$M_{\text{rec}} = \int_T^{T_0} \tau \mathrm{d}T \tag{5}$$

$$\tau = \int_{r_0}^{r_f} \sigma_{z\theta} \pi r^2 \mathrm{d}r. \tag{6}$$

Assuming axisymmetric radial deformation, shearing twist and axial extension, the displacement is

$$\boldsymbol{u} = \left[w_0 z', \ v_0 r z', \mathrm{u}(r)\right]^{\mathrm{T}} \tag{7}$$

where w_0 is the extensional strain, v_0 is the shearing strain per radius, and $u(r)$ is the unidentified radial displacement as a function of r. The mechanical strain tensor is derived by the strain–displacement relation.

$$\varepsilon = \frac{1}{2}\left(\nabla \boldsymbol{u}^{\mathrm{T}} + \nabla \boldsymbol{u}\right). \tag{8}$$

The inelastic thermal strain tensor is

$$\varepsilon_{\mathbf{th}} = \overline{\alpha} \Delta T \tag{9}$$

where $\overline{\boldsymbol{\alpha}}$ is the off-axis coefficient of thermal expansion (CTE). The stress is derived from the stress–strain relationship.

$$\boldsymbol{\sigma} = \bar{C}\left(\varepsilon - \varepsilon_{th}\right). \tag{10}$$

The bar over the CTE and elastic matrix indicate an off-axis orientation (figure 3). This is a result of the polymer buckling during the TCPA fabrication process, causing the microfibers within the polymer to rotate. Additionally, we are also applying a multi-layer analysis, which decomposes the polymer into concentric hollow cylinders. It is assumed that at each layer the microfiber rotation increases linearly, where there is no change in the microfiber angle at the center r_0 and the greatest rotation at the surface of the fiber r_N. Equation (11) is the relation

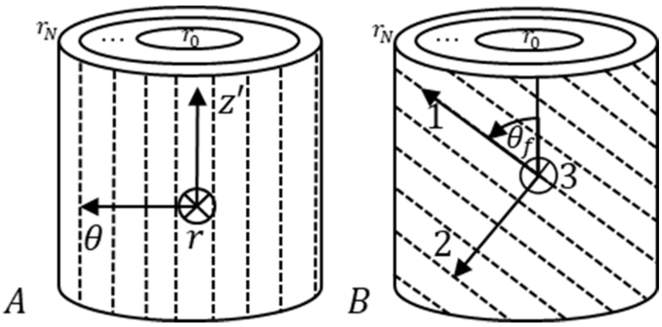

Figure 3. Multi-layer analysis with an (A) on axis frame (z', θ, r) where the microfibers are in the orientation of the polymers draw direction and (B) off axis frame (1, 2, 3) where the microfibers have rotated through angle θ_f due to buckling caused by the fabrication process.

between microfiber angle and radius, where ${\theta_f}^k$ denotes the layer whose radius is k.

$$ {\theta_f}^k = \arctan\left(\frac{k}{r_M}\tan\left(\theta_f\right)\right). \tag{11} $$

The off-axis coefficient of thermal expansion ($\overline{\alpha} = T_2\alpha$) and elastic matrix $\left(\bar{C} = T_1^T C T_2\right)$ are derived by rotating the local cylindrical coordinates about the longitudinal axis z through the angle θ_f to obtain the coordinate system denoted by 1, 2, 3 using the transformation matrices T_1 and T_2.

$$ T_1 = \begin{bmatrix} m^2 & n^2 & 0 & 0 & 0 & 2mn \\ n^2 & m^2 & 0 & 0 & 0 & -2mn \\ 0 & 0 & 1 & 0 & 0 & 0 \\ 0 & 0 & 0 & m & -n & 0 \\ 0 & 0 & 0 & n & m & 0 \\ -mn & mn & 0 & 0 & 0 & m^2-n^2 \end{bmatrix} \tag{12} $$

$$ T_2 = \begin{bmatrix} m^2 & n^2 & 0 & 0 & 0 & mn \\ n^2 & m^2 & 0 & 0 & 0 & -mn \\ 0 & 0 & 1 & 0 & 0 & 0 \\ 0 & 0 & 0 & m & -n & 0 \\ 0 & 0 & 0 & n & m & 0 \\ -2mn & 2mn & 0 & 0 & 0 & m^2-n^2 \end{bmatrix} \tag{13} $$

where $m = \cos{\theta_f}^k$ and $n = \sin{\theta_f}^k$.

For helical anisotropy for four non-zero stress and strain components, the relation was reduced.

$$ \begin{bmatrix} \sigma_z \\ \sigma_\theta \\ \sigma_r \\ \sigma_{z\theta} \end{bmatrix} = \begin{bmatrix} \bar{C}_{11} & \bar{C}_{12} & \bar{C}_{13} & \bar{C}_{16} \\ \bar{C}_{12} & \bar{C}_{22} & \bar{C}_{23} & \bar{C}_{26} \\ \bar{C}_{13} & \bar{C}_{23} & \bar{C}_{33} & \bar{C}_{36} \\ \bar{C}_{16} & \bar{C}_{26} & \bar{C}_{36} & \bar{C}_{66} \end{bmatrix} \begin{bmatrix} \varepsilon_z - \alpha_z\Delta T \\ \varepsilon_\theta - \alpha_\theta\Delta T \\ \varepsilon_r - \alpha_r\Delta T \\ \varepsilon_{z\theta} - \alpha_{z\theta}\Delta T \end{bmatrix}. \tag{14} $$

The equilibrium equations in a cylindrical configuration (figure 4) was formulated by summoning the differential stresses in the longitudinal, angular and radial directions equating to volume forces acting on the body.

$$ \frac{\partial\sigma_{rz}}{\partial r} + \frac{1}{r}\frac{\partial\sigma_{\theta z}}{\partial\theta} + \frac{\partial\sigma_z}{\partial z} + \frac{\sigma_{rz}}{r} = -F_{V_z} \tag{15} $$

$$ \frac{\partial\sigma_{r\theta}}{\partial r} + \frac{1}{r}\frac{\partial\sigma_\theta}{\partial\theta} + \frac{\partial\sigma_{\theta z}}{\partial z} + \frac{2\sigma_{r\theta}}{r} = -F_{V_\theta} \tag{16} $$

$$ \frac{\partial\sigma_r}{\partial r} + \frac{1}{r}\frac{\partial\sigma_{r\theta}}{\partial\theta} + \frac{\partial\sigma_{rz}}{\partial z} - \frac{\sigma_r - \sigma_\theta}{r} = -F_{V_r}. \tag{17} $$

By further inspection, the three equilibrium equations are simplified when considering the four non-zero stress and strain components and by noting the zero derivative terms.

$$ \frac{\mathrm{d}\sigma_r}{\mathrm{d}r} + \frac{\sigma_r - \sigma_\theta}{\mathrm{r}} = 0. \tag{18} $$

The unknown radial displacement $u(r)$ is identified by substituting the stresses into the equilibrium equation, producing a second order non-homogenous ODE

$$ \frac{\mathrm{d}^2u(r)}{\mathrm{d}r^2} + \frac{P}{r}\frac{\mathrm{d}u(r)}{\mathrm{d}r} + \frac{Q}{r^2}u(r) = R + \frac{S}{r}. \tag{19} $$

where P, Q R, and S are grouped constants. Solving the ODE gives the radial displacement

$$ u(r) = C_1 r^E + C_2 r^F + G r^2 + H r \tag{20} $$

where E, F, G, H are grouped constants and C_1 and C_2 are constants of integration. The constants of integration are obtained by applying a multi-layer analysis (figure 3). Through continuity, at each interface the displacement u and radial stress σ_r are equal and by inspection there is a no traction condition at the surface and center of the polymer, equation (21).

$$ \left\{ \begin{array}{c} \sigma_r^1(r_0) = 0 \\ \left\{ \begin{array}{l} \sigma_r^1(r_1) = \sigma_r^2(r_1) \\ u^1(r_1) = u^2(r_1) \end{array} \right. \\ \left\{ \begin{array}{l} \sigma_r^{k-1}(r) = \sigma_r^k(r) \\ u^{k-1}(r) = u^k(r) \end{array} \right. \\ \sigma_r^k(r_N) = 0 \end{array} \right. . \tag{21} $$

The superscript signifies the laminate order from 1 to k and r is the radius with at the center being r_0 and the outermost radius being r_N.

The strain components v_0 and w_0 are determined using the method of relaxation described by Pipes and Hubert [27]. With a fully defined displacement field, the strain and stress can be calculated. The thermal torque and recovery moment is defined using the stress component and the energy equation can be used to find TCPA displacement δ.

3. FEA model using COMSOL Multiphysics

An optical microscope was used to measure the dimensions of a TCPA (figure 5) fabricated from a 0.43 mm diameter nylon fiber, dimensions displayed in table 2. The TCPA was generated in COMSOL Multiphysics (figure 6). A single-coil was investigated for shorter execution time and simplicity.

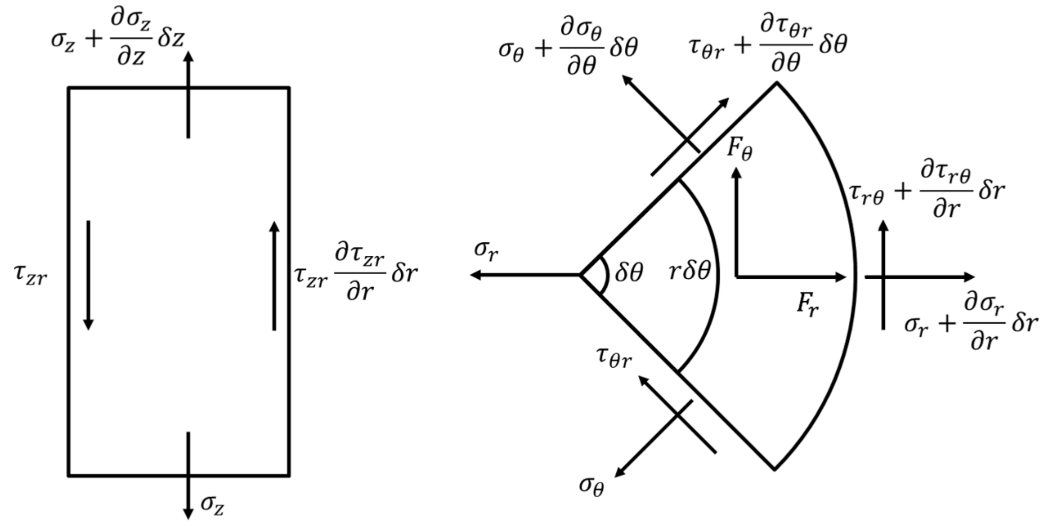

Figure 4. Differential changes of stress in a cylindrical configuration. Summation of the stress in their respective direction gives the equilibrium equations.

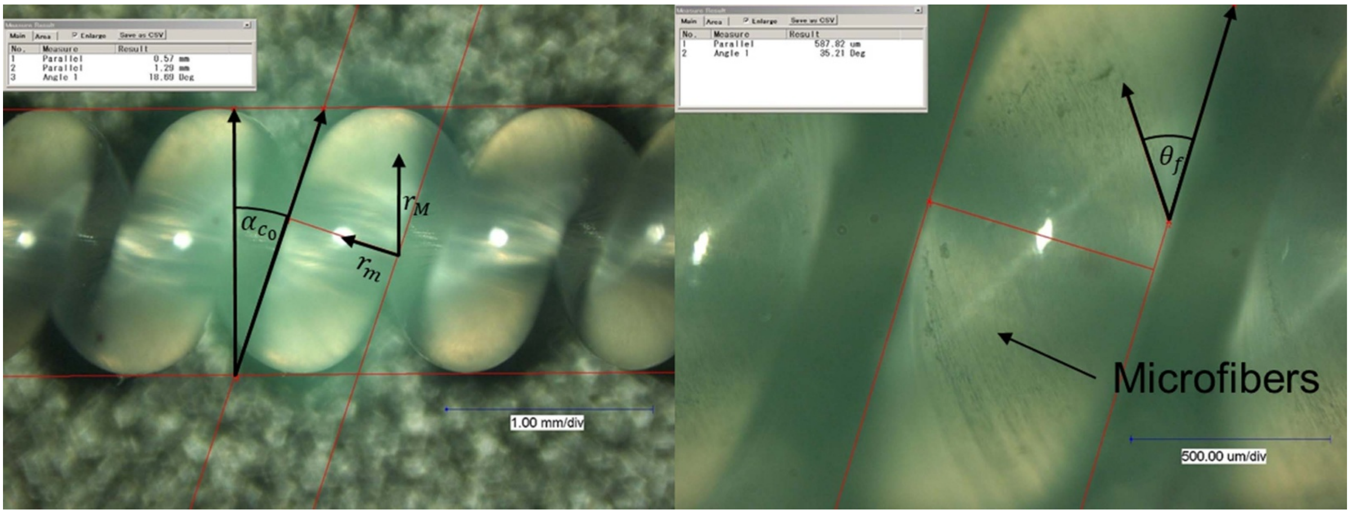

Figure 5. Optical microscope of a 0.43 mm nylon fiber fabricated into TCPA with 200 g of tension. The major and minor radius, initial bias angle and microfiber angle were measured to be utilized in the COMSOL Multiphysics simulation.

Table 2. Measured parameters obtained from an optical microscope to generate the TCPA geometry in COMSOL Multiphysics.

Parameters	Value	Description
r_{M}		Major radius (m)
r_{m}	$2.85E-4\ m$	Minor radius (m)
a_{c0}	18.69° or 0.326 rad	Initial bias angle ($^\circ$ or rad)
θ_f	35.21° or 0.615 rad	Microfiber angle ($^\circ$ or rad)

A 3D geometry increases the complexity of the model and uses a large number of elements, requiring large amounts of memory and longer run-times. Nevertheless, the investigation of a single coil is sufficient since the physics remains sound and the simulations accurately represent the thermo-mechanical response of TCPA.

To implement the material and thermal properties of the TCPA, a local cylindrical coordinate system was established in COMSOL's Curvilinear Coordinates module. This was achieved by the following coordinate transformations.

The global coordinates were transformed to local cartesian using the equation of a helix and by deriving the tangent, normal, and binormal unit vectors. The parametric equation of a helix as a function of ϕ is:

$$\vec{r_h}(\phi) = \langle b\phi, r_{\mathrm{M}}\cos\phi, r_{\mathrm{M}}\sin\phi\rangle \tag{22}$$

where b is the axial pitch of the coil, r_M is the major radius and ϕ is the angle in which the helix traces through. The tangent $\vec{t}_1$, normal $\vec{n}_1$, and binormal $\overrightarrow{\mathrm{b}_1}$ vectors were derived from the equation of the helix to formulate equation (23). Q_1 represents the transformation matrix from the global cartesian to the local

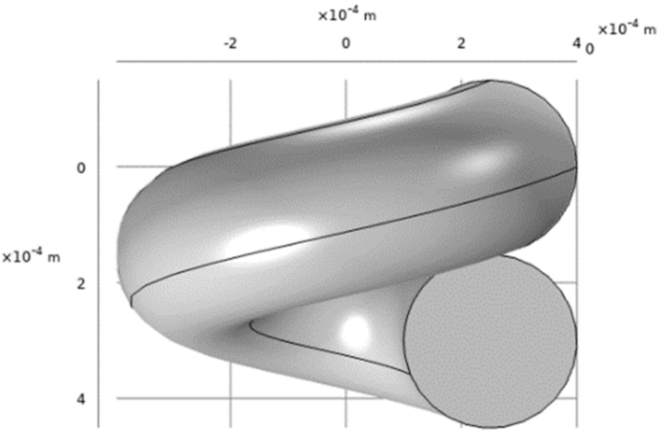

Figure 6. Geometry built in COMSOL Multiphysics of a TCPA with a major radius of 3.6E-4 m, minor radius of 2.85E-4 m and an axial pitch of 7.7E-4 m.

cartesian, where $\vec{e_1}$ is along the path of the helix and $\vec{e_2}$ and $\vec{e_3}$ are in the plane normal to the tangent.

$$\mathrm{Q}_1 = \left\{ \begin{array}{c} \vec{\mathrm{e}_1} \\ \vec{\mathrm{e}_2} \\ \vec{\mathrm{e}_3} \end{array} \right\} = \left\{ \begin{array}{c} \dfrac{\vec{t}_1}{\left|\vec{t}_1\right|} \\ \dfrac{\vec{n}_1 - \left(\vec{n}_1 \cdot \vec{e_1}\right)\vec{e_1}}{\left|\vec{n}_1 - \left(\vec{n}_1 \cdot \vec{\mathrm{e}_1}\right)\vec{\mathrm{e}_1}\right|} \\ \vec{\mathrm{e}_1} \mathrm{x} \vec{\mathrm{e}_2} \end{array} \right\}. \tag{23}$$

The non-normalized local cartesian coordinates, equations (24)–(26), are formulated for the transition from the local cartesian to local cylindrical coordinate system.

$$x' = \langle (x - x_0), (y - y_0), (z - z_0) \rangle \cdot \vec{\mathrm{e}_2} \tag{24}$$

$$y' = \langle (x - x_0), (y - y_0), (z - z_0) \rangle \cdot \vec{\mathrm{e}_3} \tag{25}$$

$$z' = \langle (x - x_0), (y - y_0), (z - z_0) \rangle \cdot \vec{\mathrm{e}_1}. \tag{26}$$

Wherein x, y, z is the spatial frame and x_0, y_0, z_0 are the spatial values at the center of the polymer. The parameterize cylindrical equation is derived using the non-normalized local cartesian coordinates, equation (27). The longitudinal direction z' does not change nor does the magnitude.

$$\vec{r} = \langle z', r_{\mathrm{m}} \cos\theta, r_{\mathrm{m}} \sin\theta \rangle \tag{27}$$

$$\theta = \mathrm{atan}\left(\frac{y'}{x'}\right). \tag{28}$$

Like equation (22), the tangent, normal, and binormal vectors are derived to obtain the second transformation matrix Q_2 for the local cylindrical coordinates, equation (29). The transformations were implemented in COMSOL's' Curvilinear Coordinate module (figure 7).

$$\mathrm{Q}_2 = \left\{ \begin{array}{c} \vec{\mathrm{e}_4} \\ \vec{\mathrm{e}_5} \\ \vec{\mathrm{e}_6} \end{array} \right\} = \left\{ \begin{array}{c} \dfrac{\vec{t}_2}{\left|\vec{t}_2\right|} \\ \dfrac{\vec{n}_2 - \left(\vec{n}_2 \cdot \vec{\mathrm{e}_4}\right)\vec{\mathrm{e}_4}}{\left|\vec{n}_2 - \left(\vec{n}_2 \cdot \vec{\mathrm{e}_4}\right)\vec{\mathrm{e}_4}\right|} \\ \vec{\mathrm{e}_4} \mathrm{x} \vec{\mathrm{e}_5} \end{array} \right\}. \tag{29}$$

The off-axis anisotropic elastic matrix $\bar{C}$ [28], CTE $\overline{\boldsymbol{\alpha}}$ [29], and displacement field $\vec{\boldsymbol{u}}$ [2] were applied in the Structural Mechanical module in the direction of the microfiber angle, using the Curvilinear Coordinates. A $F_Z = -1.6\mathrm{N}$ loading force was applied on the surface of the lower end cap and the Heat Transfer Module was used to apply a prescribed temperature $T = 23°\mathrm{C}\ -105°\mathrm{C}$ on the surface of the coil. Boundary conditions at the end caps were applied. The top end cap was constrained to allow only radial expansion and the bottom end cap was constrained to allow only global axial displacement. The displacement and von mises results are plotted in figure 8. An overall displacement δ of 0.0895 mm was observed for a single-coil TCPA as the temperature of the coil increases from 23 °C to 105 °C. The relaxation of the TCPA was not simulated due to hysteric effects, which is not the purpose of this study. Additional thermal and mechanical strain components and stress components are available as supplemental data.

4. Methods and materials

4.1. Sample preparation

The TCPA was fabricated in the lab. A fabrication apparatus was designed and constructed for the mechanical twisting of TCPA. 2.54 × 2.54 cm 80/20 T slot aluminum frames were arranged in a rectangular configuration mounted onto a metallic optical breadboard as shown in figure 9. A NEMA 23 stepper motor was used to twist the precursor fiber, which was mounted at the top end of the apparatus with the motor shaft hanging downward. SolidWorks was utilized to design the mount for the motor, a motor to precursor fiber/TCPA adapter, and a precursor fiber/TCPA to weight adapter that prevents back rotation. All parts were 3D printed from ABS plastic. The motor logic was performed by an Arduino Uno and powered with a DC power supply.

A 0.43 mm diameter commercially manufactured fishing line (Trilene®) was used as the precursor fiber for fabricating a TCPA. Approximately 200 g of tension was used to prevent snarling during the coiling process and to set the bias angle, which is weight-dependent. The fiber was twisted until the TCPA met the predetermined length of 10 mm. This length was chosen to accommodate the DMA's test section. The ends were held in place, transferred to a conventional oven, and heated to 120 °C for 30 min. The TCPA was then removed from the oven and set to cool at room temperature.

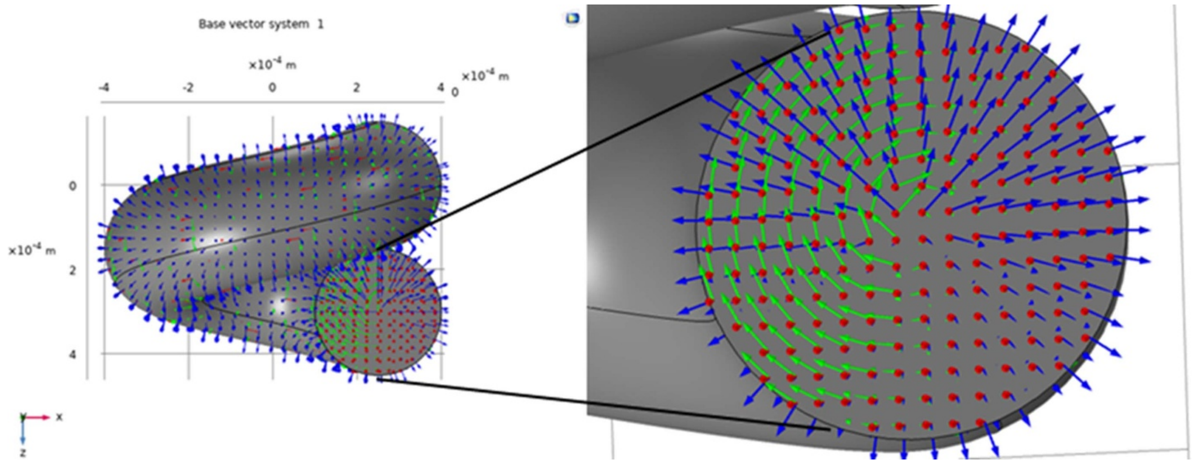

Figure 7. Local cylindrical coordinates generated using the COMSOL Multiphysics Curvilinear Coordinates module. The red, green and glue basis vectors indicate the axial, angular and radial directions.

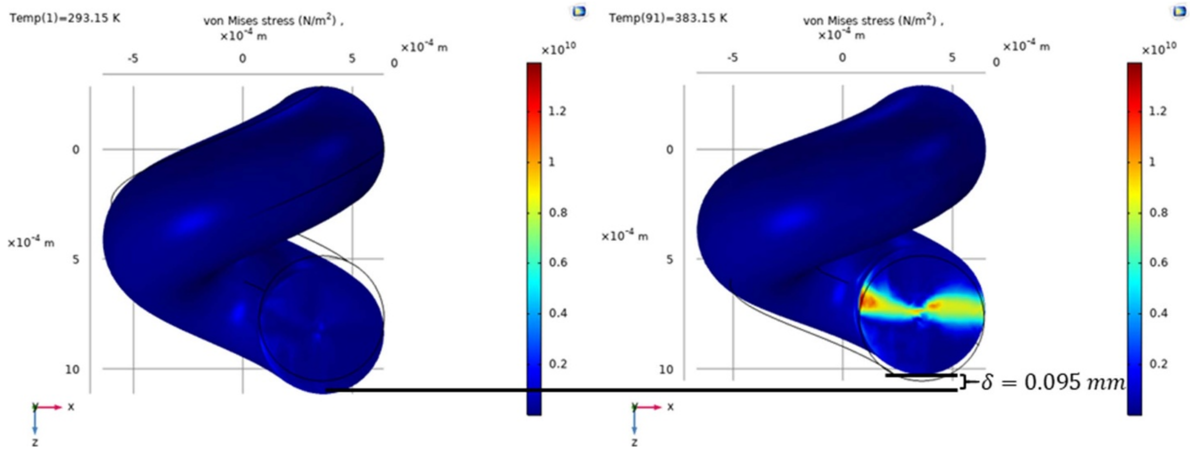

Figure 8. Von mises stress and deformation of the TCPA as temperatures increase from 23 °C to 105 °C.

4.2. Testing of the thermo-mechanical actuation response using a DMA

The thermo-mechanical response of the TCPA was measured using a Pyris Diamond DMA (figure 10), which is capable of accurate measurements of the position with a force and thermal loading. An oscillatory force is applied at a prescribed frequency and temperature range, and the resulting displacement of the material is measured. The DMA is a very sensitive measurement technique that yielded valuable thermo-mechanical data from the TCPA.

A 10 mm TCPA is placed in the sampling area of the DMA, between the two tension attachment clamps (chuck), shown in figure 11. The TCPA is adjusted with tweezers to ensure they are aligned vertically. The hex screws were then tightened to fasten both clamps and the heat shield was closed around the sample. The measurement conditions for measuring the thermo-mechanical response of TCPA were set using the DMA software. A temperature ramp was programmed from 23 °C to 105 °C with a heating rate of $3\,^{\circ}\mathrm{C\,min}^{-1}$, where $2-3\,^{\circ}\mathrm{C\,min}^{-1}$ is a commonly accepted heating rate. A force of 1.6 N was applied with an oscillation frequency of 1 Hz. These settings are summarized in table 3.

5. Results and discussion

The numerical simulation of the thermo-mechanical displacement of TCPA using COMSOL Multiphysics showed good agreement with the experimental displacement results (figure 12). The TCPA simulation was subjected to similar conditions as was experienced in the experimental test. Equal tensile load and temperature input were applied. Fort this study, only the contraction of the TCPA was tested due to hysteric effects during relaxation. Five DMA displacement measurements were taken, where the mean and standard deviations were plotted and compared to the numerical simulation. The displacement profiles were similar in magnitude and shape. The simulation had an overall displacement of 0.0895 mm were as the experimental is about 0.0738 mm and both take on a negative parabolic curve. Errors that occurred were possibly

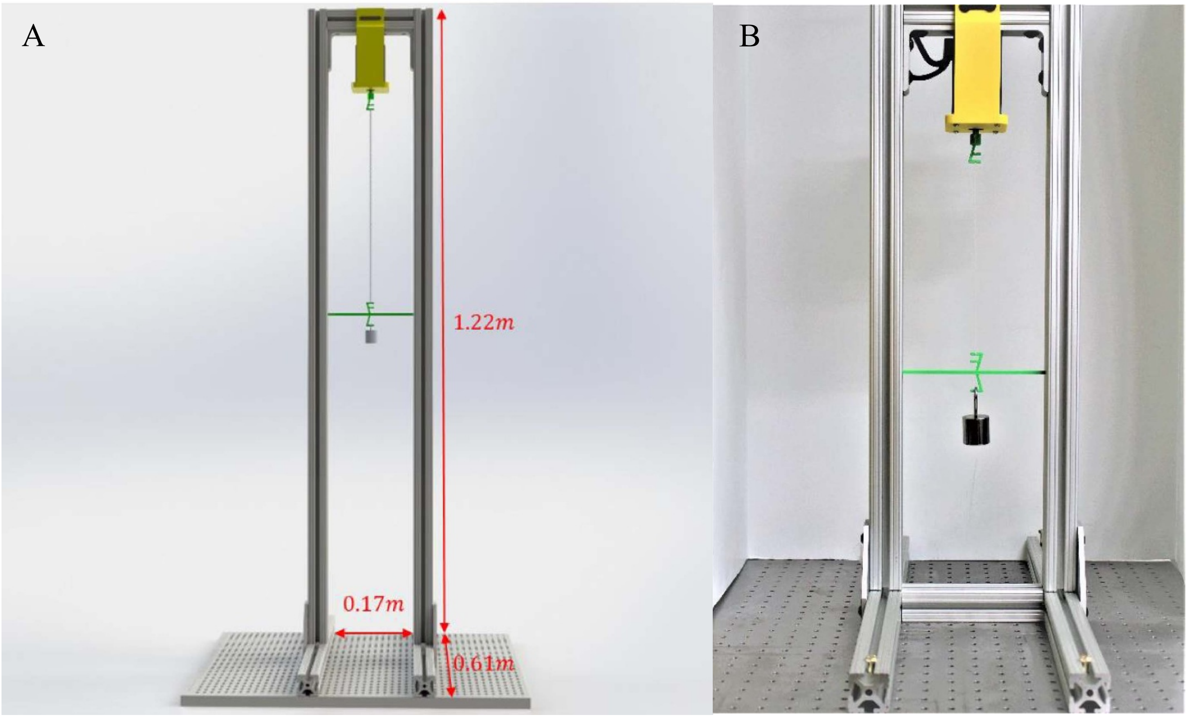

Figure 9. (A) SolidWorks rendering and (B) the constructed fabrication device used to mechanically twist polymer fibers into coils. A NEMA23 stepper motor is mounted vertically and attaches to the polymer fiber at the top. The bottom of the polymer is held taught with a 200 g mass to prevent snarling and the back rotation is prevented by the green 3D printed bar.

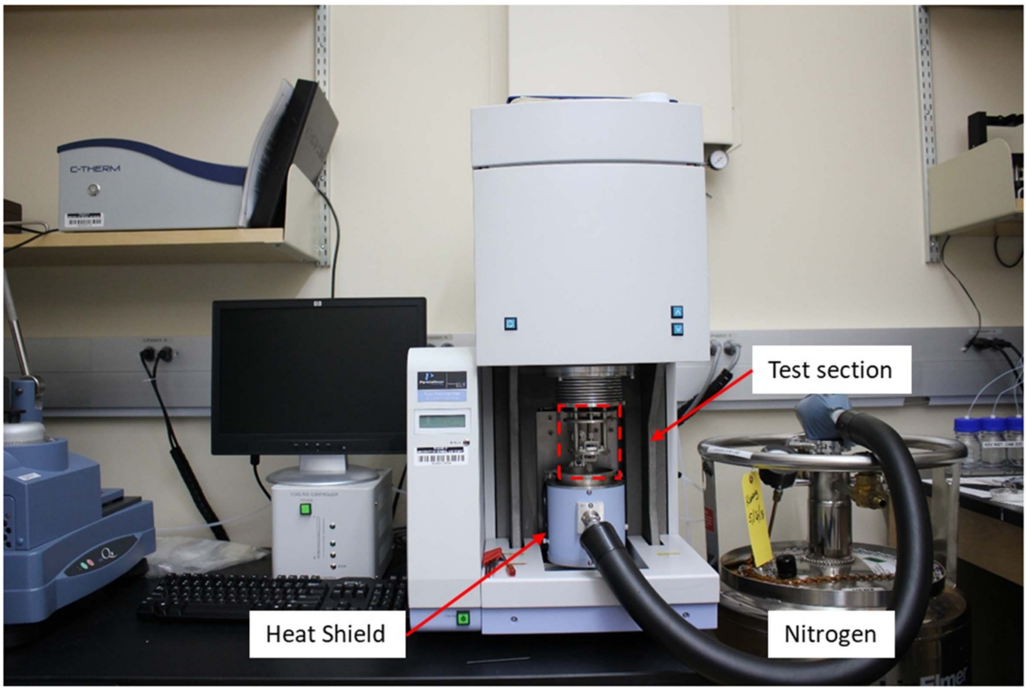

Figure 10. Pyris Diamond DMA used to measure the displacement of TCPA from 23 °C to 105 °C. A 10 mm sample of TCPA is placed in the test section, the heat shield closes over the sample where the sample is subjected to a prescribed thermal and tensile load.

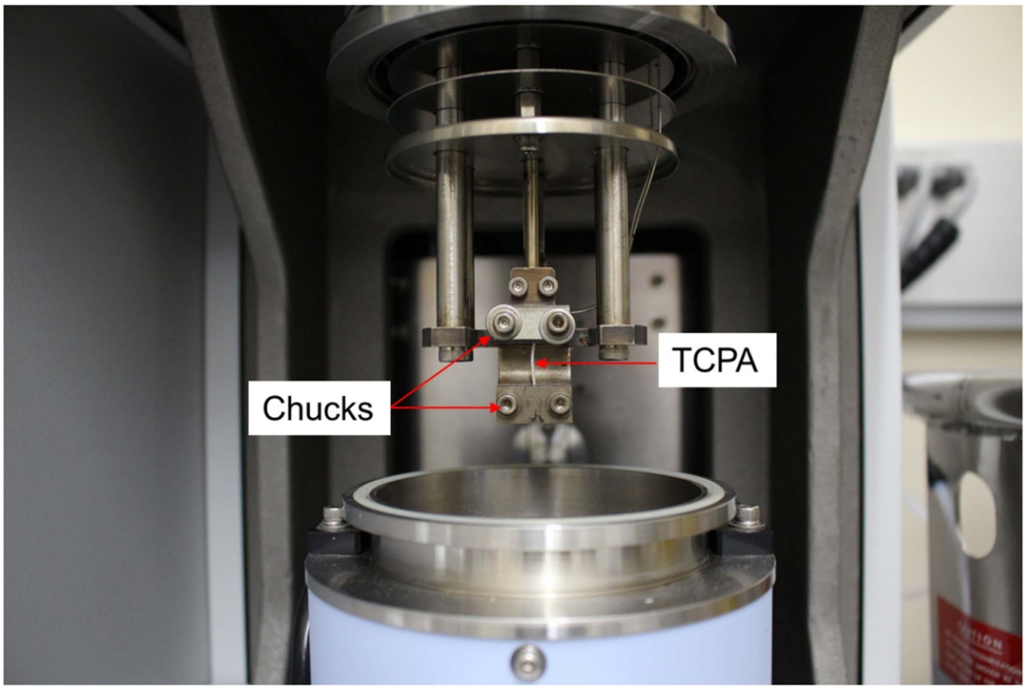

Figure 11. Test section of the DMA. The TCPA is aligned vertically in the testing section and the ends are placed in the attachment clamps (chucks).

Table 3. DMA settings for testing TCPA's thermo-mechanical response.

Temperature T	Temperature rate	Loading force	Loading force rate
23 °C – 105 °C	3 °C min^{-1}	1.6 N	1 Hz

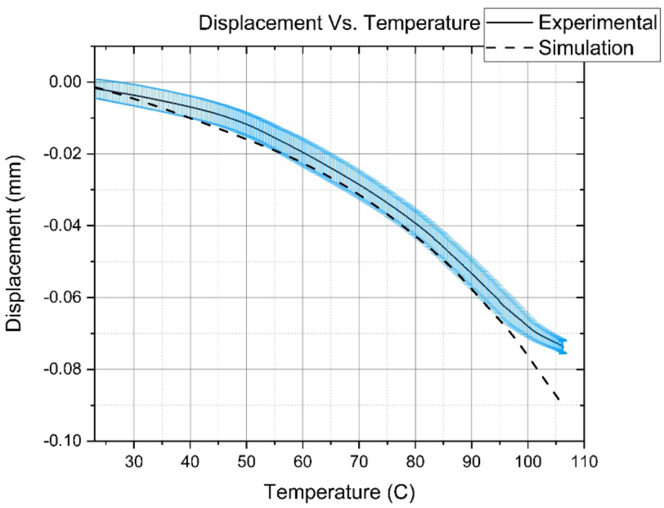

Figure 12. Comparison between the simulation and experimental displacement as the temperature increases from 23 °C to 105 °C. The average of five displacement measurements were plotted, black line, with the standard deviation, blue error bars.

due to the material and thermal properties of the polymer used in the simulation. The assumption that the elastic matrix $\bar{C}$ is constant with temperature results in error in the simulation. Also, the simulation does not model the contact forces of the coils, which limits the actuation to the axial pitch. This is seen in the simulation where the coils intersect each other causing an overshoot in displacement. Contact forces would need to be implemented to limit this phenomenon. Further investigation of the mechanical properties could decrease error, nevertheless, the results are promising. The goal of the thermo-mechanical simulation was met, providing a baseline for creating a numerical simulation for modeling the TCPA. The model can be expanded into multiple coils and be implemented in complex systems to predict the behavior of robotic systems.

6. Conclusion

Utilizing the top-down multiscale model of TCPAs created by Yang *et al* to describe the off-axis elastic and thermal expansion behavior, this study develops a first-of-its-kind 3D FEA model for the thermo-mechanical behavior of TCPAs using COMSOL Multiphysics. The new FEA model increases the adaptability of Yang's approach, where the introduction of variables can be easily implemented in the Multiphysics environment and computationally handled by computer and software. The simulation showed robust performance and indicated accurate results verified by comparison to the performance of an in-lab fabricated TCPA of similar dimensions, material properties, and loading conditions. The displacement profile of the simulation similar in magnitude and shape to that of the experimental results. By changing the input parameters, TCPA of varying material, dimensions, and loading conditions can be simulated or incorporated into multi-body simulations. This provides future researchers the capability to incorporate physics-based FEA models of TCPAs into novel robotic designs. Furthermore, future work in the FEA development may focus on extending the model to thermally expanding actuators, torsional actuators, multi-coil actuators and utilized in applications such as those seen in artificial muscles and arm prosthetics.

Data availability statement

The data that support the findings of this study are available upon reasonable request from the authors.

Acknowledgments

Authors acknowledge partial financial support from the US National Science Foundation (NSF), Partnerships for International Research and Education (PIRE) Program, Grant No. 1545857. Any opinions, findings, and conclusions or recommendations expressed in this material are those of the author(s) and do not necessarily reflect the views of the NSF.

ORCID iDs

Zakai Olsen https://orcid.org/0000-0002-4499-6677
Kwang Kim https://orcid.org/0000-0003-2134-4964

References

[1] Haines C S *et al* 2014 Artificial muscles from fishing line and sewing thread *Science* **343** 868–72
[2] Yang Q and Li G 2016 A top-down multi-scale modeling for actuation response of polymeric artificial muscles *J. Mech. Phys. Solids* **92** 237–59
[3] Yang S Y, Cho K H, Kim Y, Song M-G, Jung H S, Yoo J W, Moon H, Koo J C, Nam J-D and Choi H R 2017 High performance twisted and coiled soft actuator with spandex fiber for artificial muscles *Smart Mater. Struct.* **26** 1–9
[4] Higueras-Ruiz D R, Feigenbaum H P and Shafer M W 2020 Moisture's significant impact on twisted polymer actuation *Smart Mater. Struct.* **29** 125009
[5] Tang X, Li K, Liu Y, Zhou D and Zhao J 2019 A general soft robot module driven by twisted and coiled actuators *Smart Mater. Struct.* **28** 1–13
[6] Cho K H, Kim Y, Yang S Y, Kim K, Park J H, Rodrigue H, Moon H, Koo J C, Nam J-D and Choi H R 2019 Artificial musculoskeletal actuation module driven by twisted and coiled soft actuators *Smart Mater. Struct.* **28** 1–10
[7] Saharan L, De Andrade M J, Saleem W, Baughman R H and Tadesse Y 2017 IGrab: hand orthosis powered by twisted and coiled polymer muscles *Smart Mater. Struct.* **26** 1–14
[8] Hamidi A, Almubarak Y, Rupawat Y M, Warren J and Tadesse Y 2020 Poly-Saora robotic jellyfish: swimming underwater by twisted and coiled polymer actuators *Smart Mater. Struct.* **29** 1–16
[9] Wu L, De Andrade M J, Saharan L K, Rome R S, Baughman R H and Tadesse Y 2017 Compact and low-cost humanoid hand powered by nylon artificial muscles *Bioinsp. Biomim.* **12** 026004
[10] Kaneko Y *et al* 2016 Power-efficient low-temperature woven coiled fibre actuator for wearable applications *Sci. Rep.* **6** 1–9
[11] Sutton L, Moein H, Rafiee A, Madden J D W and Menon C 2016 Design of an assistive wrist orthosis using conductive nylon actuators *2016 6th IEEE Int. Conf. on Biomedical Robotics and Biomechatronics (Biorob)* (*July 2016*) pp 1074–9
[12] Kim S H *et al* 2015 Harvesting temperature fluctuations as electrical energy using torsional and tensile polymer muscles *Energy Environ. Sci.* **8** 3336–44
[13] Karami F and Tadesse Y 2017 Modeling of twisted and coiled polymer (TCP) muscle based on phenomenological approach *Smart Mater. Struct.* **26** 1–12
[14] Masuya K, Ono S, Takagi K and Tahara K 2018 Feedforward control of twisted and coiled polymer actuator based on a macroscopic nonlinear model focusing on energy *IEEE Robot. Autom. Lett.* **3** 1824–31
[15] Yip M C and Niemeyer G 2017 On the control and properties of supercoiled polymer artificial muscles *IEEE Trans. Robot.* **33** 689–99
[16] Takagi K, Arakawa T, Takeda J, Masuya K, Tahara K and Asaka K 2017 Position control of twisted and coiled polymer actuator using a controlled fan for cooling *Electroactive Polymer Actuators and Devices (EAPAD) 2017 (April 2017)* vol 10163 p 101632V
[17] Yip M C and Niemeyer G 2015 High-performance robotic muscles from conductive nylon sewing thread *2015 IEEE Int. Conf. on Robotics and Automation (ICRA)* pp 2313–8
[18] Tang X, Li K, Chen W, Zhou D, Liu S, Zhao J and Liu Y 2019 Temperature self-sensing and closed-loop position control of twisted and coiled actuator *Sens. Actuators* A **285** 319–28
[19] Simeonov A, Henderson T, Lan Z, Sundar G, Factor A, Zhang J and Yip M 2018 Bundled super-coiled polymer artificial muscles: design, characterization, and modeling *IEEE Robot. Autom. Lett.* **3** 1671–8
[20] Suzuki M and Kamamichi N 2018 Displacement control of an antagonistic-type twisted and coiled polymer actuator *Smart Mater. Struct.* **27** 035003
[21] Suzuki M and Kamamichi N 2018 Control of twisted and coiled polymer actuator with anti-windup compensator *Smart Mater. Struct.* **27** 1–9
[22] Suzuki M and Kamamichi N 2018 Robust control with disturbance observer for twisted and coiled polymer actuator *Smart Mater. Struct.* **27** 1–9
[23] Cho K H *et al* 2016 Fabrication and modeling of temperature-controllable artificial muscle actuator *2016 6th IEEE Int. Conf. on Biomedical Robotics and Biomechatronics (Biorob)* (*July*) vol 2016 pp 94–98
[24] Zhang J, Iyer K, Simeonov A and Yip M C 2017 Modeling and inverse compensation of hysteresis in supercoiled polymer artificial muscles *IEEE Robot. Autom. Lett.* **2** 773–80
[25] Pagano N J and Whitney J M 1970 Geometric design of composite cylindrical characterization specimens *J. Compos. Mater.* **4** 360–78
[26] Pipes R B and Hubert P 2003 Helical carbon nanotube arrays: thermal expansion *Compos. Sci. Technol.* **63** 1571–9
[27] Pipes R B and Hubert P 2002 Helical carbon nanotube arrays: mechanical properties *Compos. Sci. Technol.* **62** 419–28
[28] Tashiro K, Kobayashi M and Tadokoro H 1978 Calculation of three-dimensional elastic constants of polymer crystals. 1. Method of calculation *Macromolecules* **11** 908–13
[29] Choy C L, Chen F C and Young K 1981 Negative thermal expansion in oriented crystalline polymers *Polymer Physics Edition* **19** 335–52